NASA/TP-2003-212159

A Finite Rate Chemical Analysis of Nitric Oxide Flow Contamination Effects on Scramjet Performance

Karen F. Cabell and Kenneth E. Rock
Langley Research Center, Hampton, Virginia

May 2003

The NASA STI Program Office . . . in Profile

Since its founding, NASA has been dedicated to the advancement of aeronautics and space science. The NASA Scientific and Technical Information (STI) Program Office plays a key part in helping NASA maintain this important role.

The NASA STI Program Office is operated by Langley Research Center, the lead center for NASA's scientific and technical information. The NASA STI Program Office provides access to the NASA STI Database, the largest collection of aeronautical and space science STI in the world. The Program Office is also NASA's institutional mechanism for disseminating the results of its research and development activities. These results are published by NASA in the NASA STI Report Series, which includes the following report types:

- TECHNICAL PUBLICATION. Reports of completed research or a major significant phase of research that present the results of NASA programs and include extensive data or theoretical analysis. Includes compilations of significant scientific and technical data and information deemed to be of continuing reference value. NASA counterpart of peer-reviewed formal professional papers, but having less stringent limitations on manuscript length and extent of graphic presentations.

- TECHNICAL MEMORANDUM. Scientific and technical findings that are preliminary or of specialized interest, e.g., quick release reports, working papers, and bibliographies that contain minimal annotation. Does not contain extensive analysis.

- CONTRACTOR REPORT. Scientific and technical findings by NASA-sponsored contractors and grantees.

- CONFERENCE PUBLICATION. Collected papers from scientific and technical conferences, symposia, seminars, or other meetings sponsored or co-sponsored by NASA.

- SPECIAL PUBLICATION. Scientific, technical, or historical information from NASA programs, projects, and missions, often concerned with subjects having substantial public interest.

TECHNICAL TRANSLATION. English-language translations of foreign scientific and technical material pertinent to NASA's mission.

Specialized services that complement the STI Program Office's diverse offerings include creating custom thesauri, building customized databases, organizing and publishing research results . . . even providing videos.

For more information about the NASA STI Program Office, see the following:

- Access the NASA STI Program Home Page at ***http://www.sti.nasa.gov***

- Email your question via the Internet to help@sti.nasa.gov

- Fax your question to the NASA STI Help Desk at (301) 621-0134

- Telephone the NASA STI Help Desk at (301) 621-0390

- Write to:
  NASA STI Help Desk
  NASA Center for AeroSpace Information
  7121 Standard Drive
  Hanover, MD 21076-1320

NASA/TP-2003-212159

A Finite Rate Chemical Analysis of Nitric Oxide Flow Contamination Effects on Scramjet Performance

Karen F. Cabell and Kenneth E. Rock
Langley Research Center, Hampton, Virginia

National Aeronautics and
Space Administration

Langley Research Center
Hampton, Virginia 23681-2199

May 2003

Available from:

NASA Center for AeroSpace Information (CASI)
7121 Standard Drive
Hanover, MD 21076-1320
(301) 621-0390

National Technical Information Service (NTIS)
5285 Port Royal Road
Springfield, VA 22161-2171
(703) 605-6000

Abstract

The level of nitric oxide contamination in the test gas of the Langley Research Center Arc-Heated Scramjet Test Facility and the effect of the contamination on scramjet test engine performance were investigated analytically. A finite rate chemical analysis was performed to determine the levels of nitric oxide produced in the facility at conditions corresponding to Mach 6 to 8 flight simulations. Results indicate that nitric oxide levels range from one to three mole percent, corroborating previously obtained measurements. A three-stream combustor code with finite rate chemistry was used to investigate the effects of nitric oxide on scramjet performance. Results indicate that nitric oxide in the test gas causes a small increase in heat release and thrust performance for the test conditions investigated. However, a rate constant uncertainty analysis suggests that the effect of nitric oxide ranges from no net effect, to an increase of about 10 percent in thrust performance.

Introduction

The Langley Research Center Arc-Heated Scramjet Test Facility (AHSTF) has been used as a hypersonic air-breathing propulsion test facility since 1976. As with other high speed propulsion facilities (e.g., combustion-heated, shock-heated), the test gas is contaminated as a consequence of heating air to achieve the stagnation enthalpy necessary for flight Mach number simulation. In the AHSTF, a portion of the incoming air is heated by an electric arc to an average static temperature near 4400 K. At this temperature, air becomes partially dissociated and significant levels of atomic oxygen and nitrogen oxides (NO_x) exist. Further processing of the facility air (by mixing with unheated air and by expansion) allows the atomic oxygen to recombine upstream of the test section; however, small amounts of NO_x, primarily in the form of nitric oxide (NO), remain in the test gas.

Nitric oxide contamination is a concern in scramjet engine testing because any deviation in the composition of the test gas from atmospheric air may affect combustion and engine thrust performance. Therefore, for the results of AHSTF engine tests to be interpreted in terms of flight in atmospheric air, it is necessary to account for the effects of NO in the test gas. One effect is to reduce the amount of oxygen available for reaction with the fuel, thereby diminishing combustion heat release. Conversely, studies have shown that under certain conditions, NO can enhance combustion heat release (refs. 1 and 2). The ultimate effect of NO contamination in the AHSTF must be investigated for the NO levels and test conditions unique to the facility.

In addition to nitric oxide, other flow contaminants are present in arc-heated facilities, as addressed in reference 3. Of these other flow contaminants, copper vapor, which is released at the arc attachment points inside the heater, can be significant. The possibility of copper catalyzing the recombination of free radicals in hydrogen-air combustion is a concern (refs. 3 and 4). The authors of reference 3 report a maximum measured copper vapor level for the AEDC HEAT-H1 arc heater (under conditions similar to those in the AHSTF) to be 90 ppm mole fraction. Using an assumed reaction mechanism and catalytic efficiency for the $H + H + Cu \rightarrow H_2 + Cu$ reaction, they predicted the 90 ppm mole fraction of Cu to cause an 11-percent reduction in the reaction time of stoichiometric hydrogen-air combustion (at an initial pressure and temperature of 0.19 atm and 1390 K). However, the experimental measurements of reference 4 show that copper in concentrations up to 10^{-6} mole fraction has no catalytic effect on $H_2 + O_2 + N_2$ flames (at atmospheric pressure and a 1800–2500 K temperature range). The copper vapor produced in

the AHSTF has never been measured and neither its effect on NO_x production nor on scramjet engine combustion is known at this time. The present study assumes that the possible effects of Cu and NO are independent and addresses only the effects of NO.

This paper presents an analysis in two parts. In the first part, a one-dimensional finite rate chemistry code was used to analyze the flow through each component of the AHSTF over a range of operating conditions corresponding to Mach 6, 7, and 8 flight simulations. A six-reaction mechanism for dissociated air was employed. The air composition was computed at discrete stations up to the test section entrance where calculated NO levels were compared with experimentally measured levels. The present report expands on the work of reference 5 in that NO levels were analytically quantified over a larger range of facility operating conditions.

The second part of the analysis models the reacting flow through a representative test engine flow path. A one-dimensional, three-stream code with finite-rate chemistry was used to model the engine combustor and nozzle flow segments. A 68-reaction air-hydrogen-silane mechanism was used for the combustion process. The engine flow path analysis focused on the Mach 8 flight simulation using fuel equivalence ratios of 0.5, 1.0, and 1.5. An investigation of the effect of NO contamination was made by comparing calculated engine performance for NO-contaminated air with that for nondissociated atmospheric air. The work of reference 5 was expanded by providing a more detailed investigation of the role of NO in the combustion chemistry. Also, to investigate the sensitivity of the results to uncertainties in the rate constants, an analysis was performed wherein rate constants of key reactions were varied within recommended error limits.

Nomenclature

A pre-exponential factor in expression for reaction rate constant, k_j

a engine flow area, cm^2

a_e engine nozzle exit area, cm^2

a_2 engine combustor entrance area, cm^2

c constant in expression for fuel-air mixing fraction, cm^{-1}

ΔF change in engine thrust from fuel-off to fuel-on conditions, N

E reaction activation energy, cal/g-mole

F sum of wall pressure and skin friction axial forces on engine combustor and nozzle, N

f uncertainty factor in reaction rate constant

$h_{t,\infty}$ flight stagnation enthalpy and facility stagnation enthalpy, kJ/kg

k_j forward reaction rate constant for reaction j; cm^3/g-mole for bimolecular reactions, $cm^6/(\text{g-mole})^2$ for termolecular reactions

M_1 Mach number at facility nozzle exit/engine entrance plane

M_∞ flight Mach number

$\dot{m}_a$ mass flow rate of air entering engine, kg/s

$\dot{m}_f$ mass flow rate of fuel injected into engine, kg/s

n temperature exponent in expression for reaction rate constant

p static pressure, atm

p_e static pressure at engine nozzle exit plane, atm

$p_{t,1}$ stagnation pressure behind vehicle bow shock, also facility stagnation pressure, atm

p_1 static pressure at engine inlet entrance plane, atm

p_2 static pressure at engine combustor entrance plane, atm

R universal gas constant, cal/g-mole-K

T static temperature, K

$T_{t,\infty}$ free-stream stagnation temperature, K

V velocity, m/s

V_e velocity at engine nozzle exit plane, m/s

V_2 velocity at engine combustor entrance plane, m/s

η_m fuel-air mixing fraction

ϕ fuel to total oxygen equivalence ratio

ϕ_{H_2} hydrogen equivalence ratio

ϕ_{sim} silane-hydrogen mixture equivalence ratio

ϕ_{tot} total fuel equivalence ratio

Facility Description

The Langley Research Center Arc-Heated Scramjet Test Facility (AHSTF) generates high energy air flows for testing airframe-integrated subscale scramjet engine modules for hypersonic vehicles. Figure 1 shows a typical hypersonic vehicle in flight and also shows the corresponding ground facility simulation for the scramjet engine. The AHSTF uses arc-heated air to duplicate true flight stagnation enthalpy conditions for a flight Mach number (M_∞) range of 4.7 to 8. The heated test gas is expanded through a

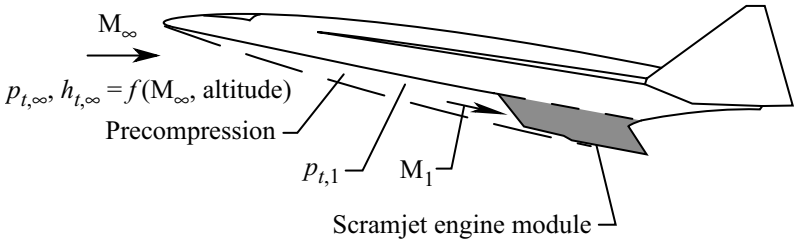

(a) Hypersonic vehicle in flight.

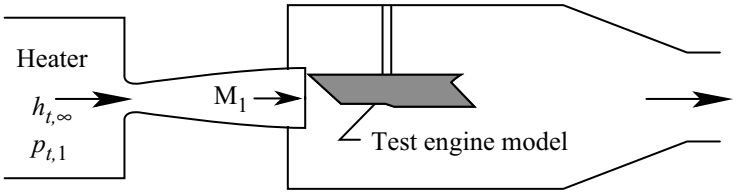

(b) Simulation in ground facility.

Figure 1. Ground test simulation of flight for scramjet engine testing.

nozzle to a Mach number M_1, providing a free-jet simulating condition behind the oblique forebody shock of a hypersonic vehicle flying at various angles of attack.

Figure 2 shows the simulation capability of the AHSTF in terms of flight altitude and Mach number. Tests can be conducted at stagnation enthalpies and pressures corresponding to the flight Mach number range and altitudes indicated by the shaded region. Also shown in figure 2, on the lower axis, is the free-stream stagnation temperature range corresponding to the test Mach number range. These temperatures, ranging from approximately 1100 to 2800 K, are produced in the stagnation region upstream from the facility nozzle expansion.

Detailed descriptions of the AHSTF are given in references 6 and 7; therefore, only the steps involved in processing the facility air are explained in this report. Figure 3 shows a schematic of the three primary components upstream from the facility test section: the arc heater, the plenum (including the plenum injector rings), and the nozzle. The arc heater is a cylindrical vessel comprised of an upstream and down-stream electrode. The air entering the heater, referred to as "main air," is heated by an electric arc that is established between the upstream and downstream electrodes. Except for the arc attachment regions, the arc is mainly confined to the centerline of the heater by the vortex flow resulting from the swirl injection of the main air. According to reference 3, in a typical arc heater about 5 percent of the total air is heated directly by the arc and becomes fully dissociated; the remainder of the air is heated relatively slowly by radiation and conduction and is dissociated to a lesser degree.

This dissociated main air then enters the plenum where unheated air is injected through the plenum injector rings, and is mixed with the main air. The ambient temperature bypass air is added in an amount necessary to achieve a mixture stagnation enthalpy, $h_{t,\infty}$, corresponding to the desired altitude and flight Mach number simulation. The bypass air is injected radially through the plenum injector rings to break up the swirling motion of the main air exiting the heater and to enhance mixing of the two air streams.

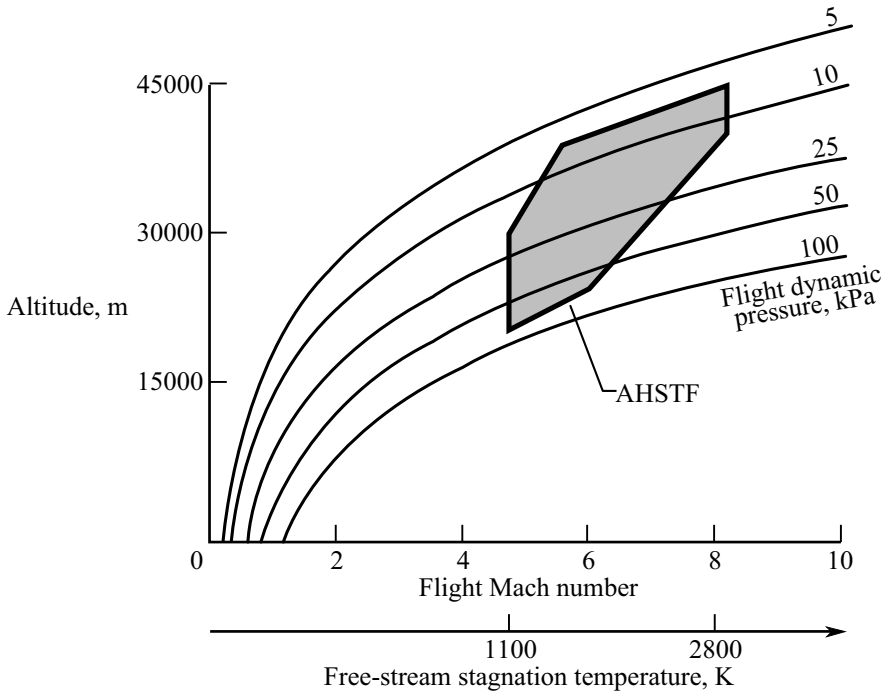

Figure 2. Simulation capability of AHSTF.

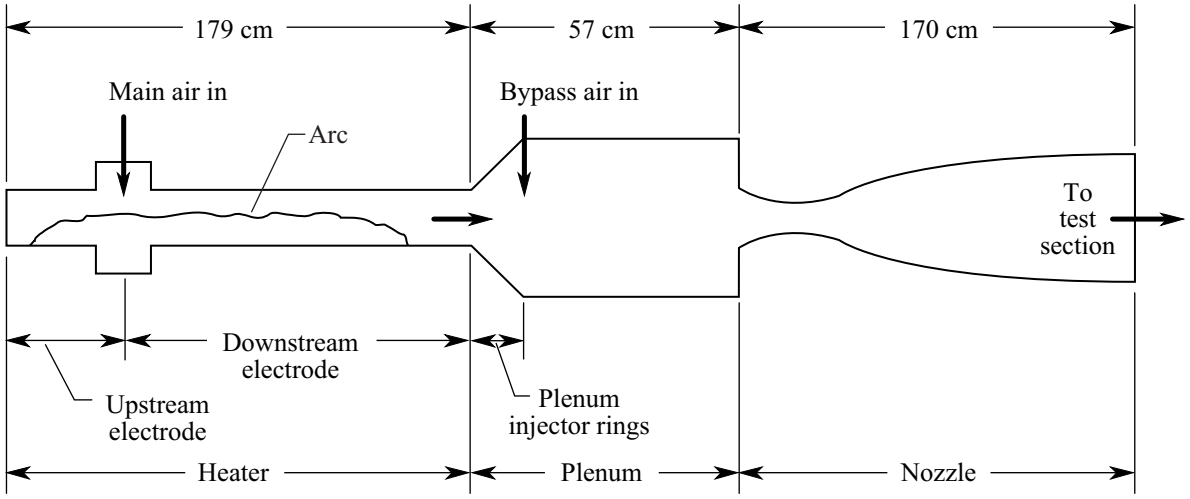

Figure 3. Schematic of facility arc heater, plenum, and nozzle.

This method of heating only a portion of the total air to elevated temperatures and then mixing it with cooler air to achieve the desired test conditions is necessary because the heater cannot operate in a stable mode while processing the full facility air flow rates. The resulting air mixture exiting the plenum is expanded through a converging/diverging supersonic nozzle and enters the test section. Two fixed geometry nozzles are available to expand the test gas to an aerodynamic Mach number (M_1) of 4.7 or 6.0. For the M_∞ = 6, 7, and 8 flight simulations, the M_1 = 6 nozzle is used; thus a different level of forebody precompression is simulated for each flight Mach number.

Altitude simulation at a given flight stagnation enthalpy is achieved by varying the arc power. The AHSTF power supplies have 33 discrete power settings, referred to as tap settings, and greater power is delivered at higher tap settings. Satisfactory operation of the heater requires that main air be increased as tap setting is increased. In order to obtain the same mixture stagnation enthalpy at a higher tap setting, the bypass air flow rate must be increased accordingly. Total facility air flow rate therefore increases and higher plenum pressures are required to drive the flow through the fixed geometry nozzle. Thus, for a constant stagnation enthalpy simulation, higher tap settings produce greater air densities and therefore simulate lower altitudes.

The bulk of scramjet engine tests are conducted at the higher tap settings because they better simulate typical altitudes for hypersonic vehicle trajectories. For this reason, three upper tap settings were chosen for this study. These were taps 23 (historically the standard operating point), taps 29, and taps 33. Nominal facility operating conditions are listed in table 1 for each Mach number simulation and tap setting considered. Note that a constant Mach number simulation corresponds to a nearly constant stagnation enthalpy simulation. The values in the table demonstrate both the variation of bypass air to achieve the target stagnation enthalpy at a fixed tap setting and the variation of tap setting for simulating different altitudes at a fixed flight Mach number. The taps 33 setting at the $M_\infty = 6$ condition is not included because the resulting stagnation pressure exceeds the heater pressure limit of 45 atm; therefore, it is not an allowable operating point.

The electrodes, plenum injector rings, plenum wall, and nozzle throat are made of copper and are water cooled. During a test, the heat transferred from the walls of each of these components is deduced from an energy balance on the cooling water to each component. Table 2 provides typical values of the component heat losses for the range of operating points considered here. These values were used in the analysis described subsequently.

Table 1. AHSTF Nominal Operating Conditions

[Estimated uncertainties for directly measured or experimentally derived quantities are as follows: arc power: ±1 percent, main air: ±1.7 percent, bypass air: ±1.5 percent, $p_{t,1}$: ±0.3 percent, $h_{t,\infty}$: ±2.9 percent]

Condition	Nominal operating conditions for—							
	$M_\infty = 6$ flight simulation		$M_\infty = 7$ flight simulation			$M_\infty = 8$ flight simulation		
	Taps 23	Taps 29	Taps 23	Taps 29	Taps 33	Taps 23	Taps 29	Taps 33
Altitude, m	27 005	25 664	35 357	33 863	32 979	42 398	40 874	40 234
Arc power, MW	9.40	11.45	9.40	11.45	12.75	9.40	11.45	12.75
Main air, kg/s	0.72	0.88	0.72	0.88	0.99	0.72	0.88	0.99
Bypass air, kg/s	2.19	2.71	1.32	1.66	1.88	0.71	0.92	1.04
$p_{t,1}$, atm	35.1	43.2	28.6	35.1	39.7	23.0	28.3	31.9
$h_{t,\infty}$, kJ/kg	1 837	1828	2570	2524	2500	3552	3459	3403
$T_{t,\infty}$, K	1 667	1661	2251	2217	2203	2860	2825	2804

Table 2. AHSTF Component Heat Losses as Fraction of Arc Power

Component	Heat loss fraction	Uncertainty, percent
Upstream electrode	0.11	±1.3
Downstream electrode	0.36	±1.2
Plenum injector rings	0.08	±1.8
Plenum liner	0.34	±1.6
Nozzle throat	0.30	±1.3

Part I: NO_X Concentration in the Facility

Analysis Methodology

To calculate the nitrogen oxide (NO_X) concentration in the facility, a chemical kinetics code (ref. 8) was used to model the reacting flow through each of three components (heater, plenum, and nozzle) upstream from the facility test section. The kinetics code, based on the earlier code of reference 9, models one-dimensional, adiabatic and inviscid flow. It numerically solves the governing mass, momentum and energy equations, and species continuity equations for each species present. The reactions and rate constants used to describe the air dissociation and recombination were extracted from the mechanism of reference 1 and are listed in table 3. The flow through each of the three components was analyzed individually beginning with the heater. For each component, an area distribution was specified along with entrance conditions. The entrance conditions were consistent with the known initial composition, initial pressure, fixed stagnation enthalpy, and mass flow rate for each component. The code then computed the chemical composition and fluid dynamic properties through each component up to the facility nozzle exit.

Table 3. Air Reaction Mechanism

Reaction[a]	A	n	E
$N + O_2 \rightarrow NO + O$	6.40×10^9	1.0	6 300
$N + NO \rightarrow N_2 + O$	1.60×10^{13}	0	0
$M + NO_2 \rightarrow NO + O + M$	1.16×10^{16}	0	66 000
$O + NO_2 \rightarrow NO + O_2$	1.00×10^{13}	0	600
$N + N + M \rightarrow N_2 + M$	2.80×10^{17}	−0.8	0
$O + O + M \rightarrow O_2 + M$	1.10×10^{17}	−1.0	0

[a]Forward reaction rate constants are of the form $k = AT^n e^{-E/RT}$; units are in the cgs system (see nomenclature). Third body efficiencies for all termolecular reactions are 1.0 for all M.

Before employing the kinetics code, an energy balance was performed on the heater. The stagnation enthalpy of the air at the heater exit was calculated using the main air flow rate and associated arc power (table 1) as well as the heat loss to the electrodes (table 2). With the initial air composition specified to be consistent with the ambient supply air, the code was used to model the reacting (dissociating) flow of the main air through the heater at a stagnation enthalpy matching the calculated exit enthalpy. In effect, this method assumes that the heat transfer can be modeled separately from the chemical reactions by enforcing instantaneous heat addition at a frozen composition of the ambient incoming air, then allowing reactions to take place adiabatically as the air flows through the heater. The assumption of instantaneous heat

addition was validated by an analysis that used a distributed heat addition and resulted in identical conditions at the heater exit. The flow through the heater is low subsonic (the Mach number is ≈0.1); thus, the initial static pressure was set equal to the facility stagnation pressure ($p_{t,1}$ from table 1).

A similar procedure was followed for the analysis of the plenum. The initial static pressure was again set to equal the facility stagnation pressure (here the Mach number is ≈0.01). The initial composition was assumed to result from a chemically frozen mixing of the dissociated main air and the nondissociated ambient bypass air. Reactions were then allowed to occur at a constant enthalpy equal to the plenum exit stagnation enthalpy, which was calculated from an energy balance of the plenum flow process.

For the nozzle analysis, the area distribution of the contoured converging section was assigned and the code was used to determine the stagnation enthalpy required to reach a choked condition at the prescribed stagnation pressure, mass flow rate, and throat area. If this enthalpy was not equal to that calculated from an energy balance, the computations were repeated with an adjusted heater exit enthalpy such that, with subsequent component heat losses, the nozzle throat enthalpy derived from the energy balance was equal to the enthalpy at which the nozzle choked. In the analysis of the diverging nozzle section, no further heat loss was imposed. Chemical reactions were allowed to take place at constant stagnation enthalpy equal to the throat stagnation enthalpy. Boundary layer effects were approximated by a prescribed area ratio distribution to achieve Mach 6 at the nozzle exit plane, consistent with facility measurements.

In the analysis described above, uncertainties in calculated nitric oxide (NO) levels due to uncertainties in facility conditions (e.g., arc power, air flow rates, heat losses) were not determined.

Results

Calculations show that the air dissociation that occurs in the arc heater is similar for all Mach number simulations and tap settings. This is true because the ratio of arc power to main air flow rate is approximately the same for all cases (see table 1) resulting in similar heater exit temperatures (roughly 4400 K); the differences in pressure have only a small effect. The dissociation process is illustrated in figure 4 by species concentration traces for the Mach 7, taps 23 simulation. Equilibrium is reached within 0.004 ms, which is very small relative to the heater residence times of 6 to 10 ms. The heater exit state for each flight Mach simulation and tap setting is given in table 4. The NO_x species, ranging between 8 and 9 mole percent, are primarily composed of NO with trace amounts of NO_2. A significant level (≈15 mole percent) of atomic oxygen also exits the heater.

Calculations for the plenum and nozzle flow show that both the atomic oxygen and nitric oxide concentrations are significantly reduced compared with the levels exiting the heater. Results for the plenum and nozzle flow are given in table 5, which lists the plenum and nozzle exit conditions and gas composition for each Mach number and tap setting. In all cases, the air at the nozzle exit contains no more than 0.01 mole percent of atomic oxygen and no more than 0.07 mole percent of NO_2; however, NO remains at levels up to 3 mole percent. Therefore, the remaining discussion focuses on the survival of NO.

Calculated NO concentrations throughout the heater, plenum, and nozzle are presented for comparison in figure 5 for the M_∞ = 6, 7, and 8 simulations, all at the standard taps 23 power setting. In all cases, the NO in the flow exiting the heater is initially diluted by mixing process with the bypass air (as indicated at the entrance to the plenum in fig. 5). This dilution effect is greatest for the lowest enthalpy simulation (M_∞ = 6) because it uses the most bypass air. The temperature drop due to the instantaneous mixing with the cooler bypass air places the gas in a nonequilibrium state. As the air flows through the plenum, the

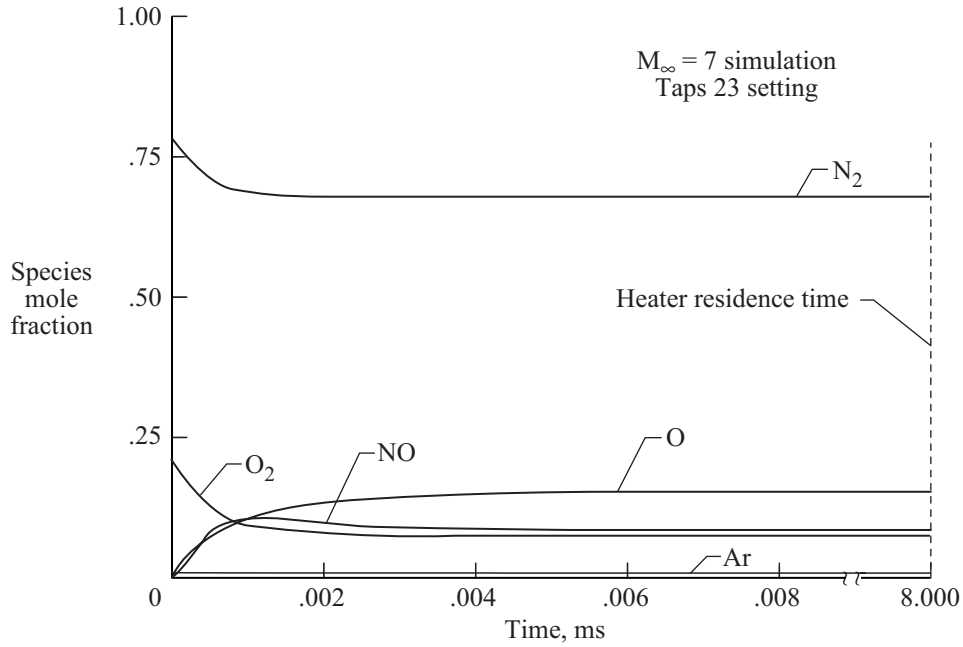

Figure 4. Air dissociation in arc heater.

Table 4. Calculated Conditions and Test Gas Composition at Heater Exit

Condition	Nominal operating conditions for—							
	M_∞ = 6 flight simulation		M_∞ = 7 flight simulation			M_∞ = 8 flight simulation		
	Taps 23	Taps 29	Taps 23	Taps 29	Taps 33	Taps 23	Taps 29	Taps 33
p, atm	35.1	43.2	28.6	35.1	39.7	23.0	28.3	31.9
T, K	4427	4483	4395	4434	4452	4316	4327	4335
Mole fractions								
N_2	0.6797	0.6792	0.6788	0.6793	0.6799	0.6806	0.6828	0.6839
O_2	0.0772	0.0773	0.0751	0.0766	0.0779	0.0770	0.0810	0.0831
N	0.0010	0.0011	0.0010	0.0010	0.0010	0.0009	0.0008	0.0008
O	0.1472	0.1449	0.1530	0.1483	0.1447	0.1518	0.1430	0.1382
NO	0.0862	0.0888	0.0834	0.0861	0.0878	0.0810	0.0837	0.0852
NO_2	0.0001	0.0001	0.0001	0.0001	0.0001	0.0001	0.0001	0.0001
Ar	0.0086	0.0086	0.0086	0.0086	0.0086	0.0086	0.0086	0.0087

Table 5. Calculated Conditions and Test Gas Composition at Plenum and Nozzle Exits

Calculated conditions and test gas composition for—						
M_∞ = 6 flight simulation						
Condition	Taps 23		Taps 29			
	Plenum exit	Nozzle exit	Plenum exit	Nozzle exit		
p, atm	35.1	0.0187	43.2	0.0231		
T, K	1614	210	1605	208		
Mole fractions						
N_2	0.7699	0.7699	0.7698	0.7698		
O_2	0.1978	0.1978	0.1976	0.1976		
N	0	0	0	0		
O	0	0	0	0		
NO	0.0225	0.0224	0.0227	0.0226		
NO_2	0.0005	0.0006	0.0006	0.0007		
Ar	0.0093	0.0093	0.0093	0.0093		
M_∞ = 7 flight simulation						
Condition	Taps 23		Taps 29		Taps 33	
	Plenum exit	Nozzle exit	Plenum exit	Nozzle exit	Plenum exit	Nozzle exit
p, atm	28.6	0.0135	35.1	0.0168	39.7	0.0190
T, K	2144	287	2106	281	2102	281
Mole fractions						
N_2	0.7702	0.7704	0.7694	0.7696	0.7693	0.7695
O_2	0.1983	0.1985	0.1975	0.1976	0.1975	0.1975
N	0	0	0	0	0	0
O	0.0002	0	0.0001	0	0.0001	0
NO	0.0218	0.0216	0.0235	0.0233	0.0236	0.0234
NO_2	0.0002	0.0002	0.0002	0.0002	0.0002	0.0003
Ar	0.0093	0.0093	0.0093	0.0093	0.0093	0.0093
M_∞ = 8 flight simulation						
Condition	Taps 23		Taps 29		Taps 33	
	Plenum exit	Nozzle exit	Plenum exit	Nozzle exit	Plenum exit	Nozzle exit
p, atm	23.0	0.0094	28.3	0.0114	31.9	0.0128
T, K	2783	389	2706	372	2687	368
Mole fractions						
N_2	0.7626	0.7659	0.7648	0.7674	0.7654	0.7677
O_2	0.1898	0.1940	0.1924	0.1955	0.1930	0.1958
N	0	0	0	0	0	0
O	0.0046	0.0001	0.0031	0	0.0027	0
NO	0.0336	0.0306	0.0303	0.0277	0.0295	0.0271
NO_2	0.0001	0.0001	0.0001	0.0001	0.0001	0.0001
Ar	0.0093	0.0093	0.0093	0.0093	0.0093	0.0093

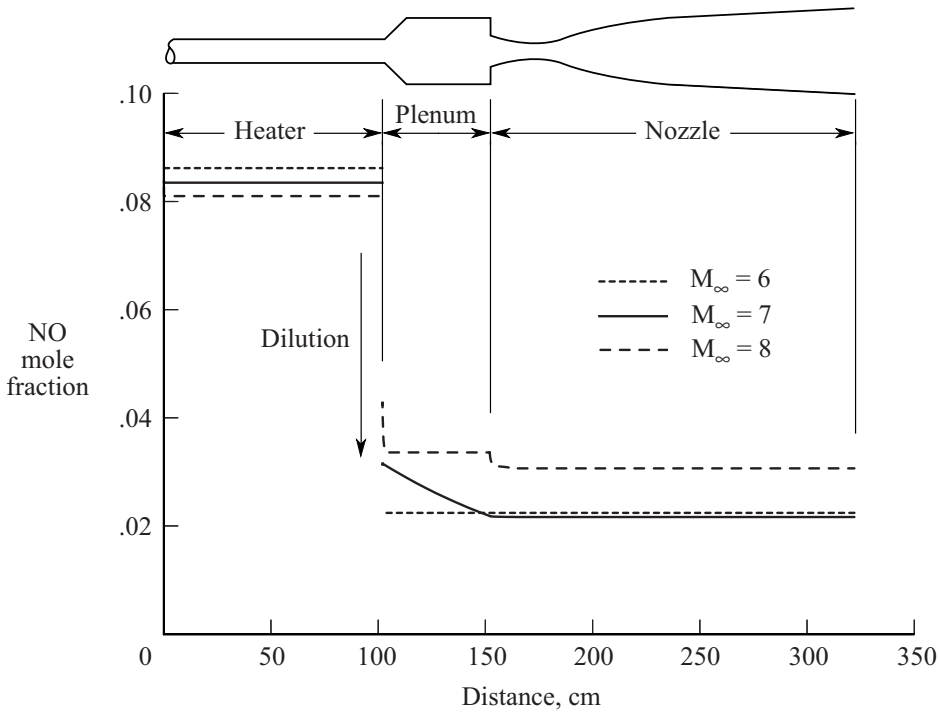

Figure 5. Calculated NO levels for M_∞ = 6, 7, and 8 simulations, standard taps 23 setting.

dissociated species recombine and the static temperature increases. However, the level of reactivity is dependent on the extent of the initial cooling. Because more bypass air is used for a lower Mach number simulation, more cooling takes place, resulting in a lower mixture temperature and a less reactive flow. The subsequent discussion considers each Mach number simulation in turn.

The calculated NO levels for the Mach 6 enthalpy simulations are shown in figure 6. For both the taps 23 and 29 settings, mixing with the bypass air dilutes the NO to slightly greater than 2 mole percent and reduces the temperature to about 1300 K. As the air flows through the plenum, initial recombination of atomic oxygen and nitrogen takes place and the temperature increases to about 1600 K, but this temperature is too low for noticeable changes in composition within the plenum residence time. The NO remains at the diluted level of about 2.3 mole percent compared with less than 1 mole percent in air at equilibrium at the plenum pressures and enthalpies. As the temperature decreases further through the facility nozzle, the composition remains essentially frozen for both Mach 6 enthalpy cases.

Results for the Mach 7 enthalpy simulations are shown in figure 7. For these cases, which use less bypass air compared with the Mach 6 cases, the process of mixing with bypass air dilutes the NO to approximately 3 mole percent and reduces the temperature to about 1700 K. As the air flows through the plenum, it is more reactive compared with the Mach 6 condition due to a higher mixture temperature (which reaches about 2100 K as the species recombine); however, reactions are too slow to yield an equilibrium composition. Slightly lower temperatures (see table 5) for the taps 29 and 33 settings, compared with taps 23, result in slightly less reactivity and this is the main reason for the differences seen between tap settings. The NO decreases to levels ranging from 2.2 to 2.4 mole percent compared with equilibrium levels around 1.1 percent at the plenum pressure and enthalpy for each tap setting. In the nozzle, recombination of atomic oxygen continues, but the NO level remains nearly constant. The composition freezes near the throat as the temperature decreases.

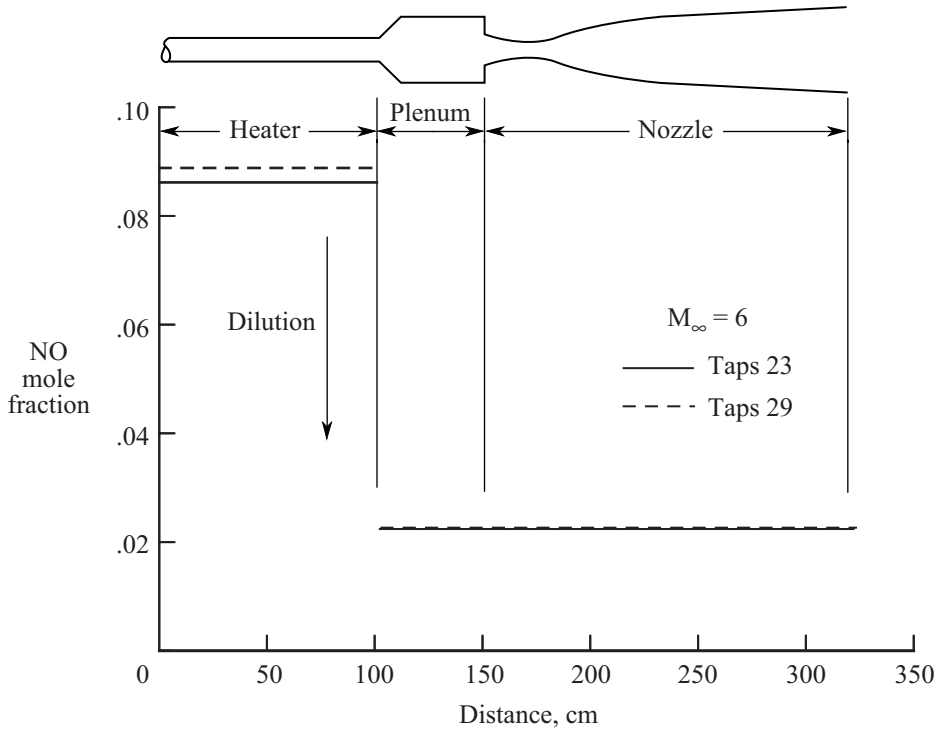

Figure 6. Calculated NO levels for Mach 6 simulations.

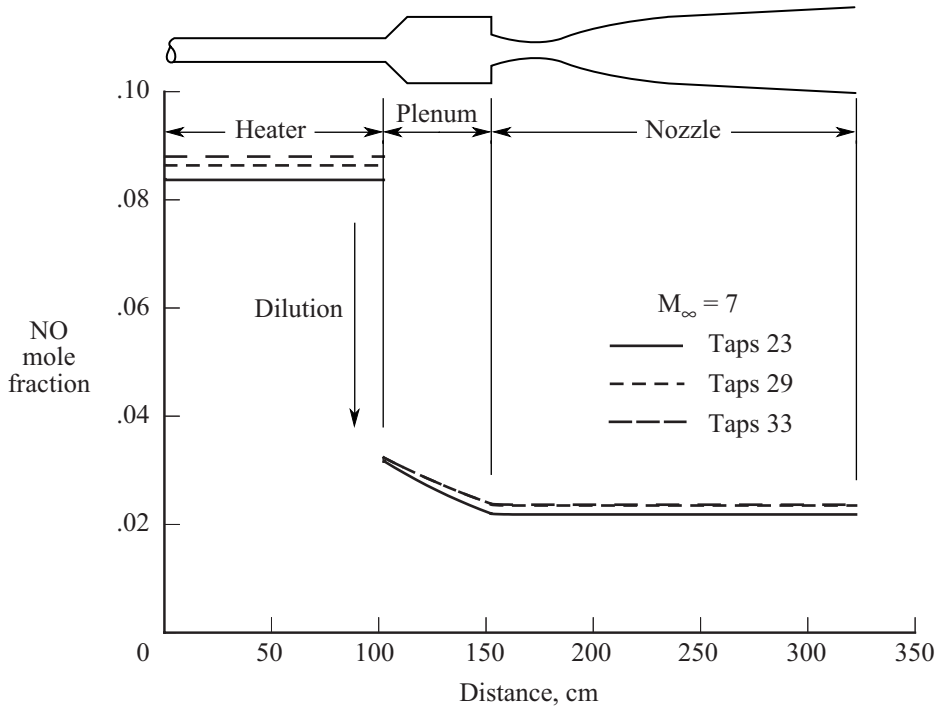

Figure 7. Calculated NO levels for Mach 7 simulations.

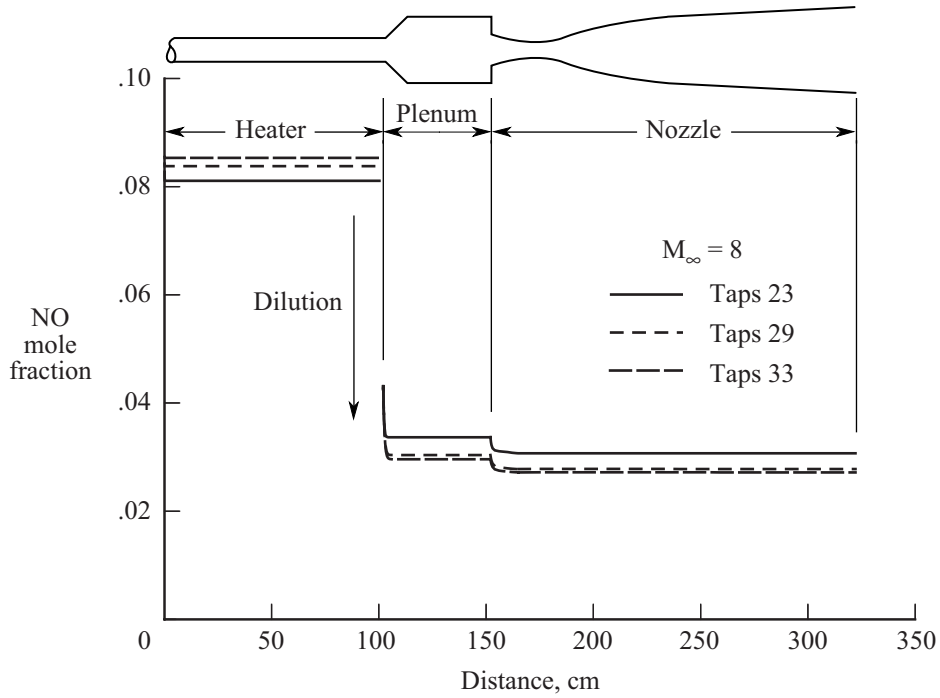

Figure 8. Calculated NO levels for Mach 8 simulations.

Results for the Mach 8 enthalpy simulations are shown in figure 8. For these cases, wherein the least bypass air is injected, the NO is diluted to 4.2 mole percent and the temperature is reduced to about 2200 K at the plenum entrance. As recombination takes place in the plenum, the temperature reaches about 2800 K. As a result of the higher temperature for the Mach 8 cases (compared with the Mach 6 and 7 cases), reactions are fast enough to yield an equilibrium composition in the plenum. The NO decreases rapidly to equilibrium levels ranging from 3.0 to 3.4 mole percent. Slightly lower temperatures for the taps 29 and 33 settings (compared with taps 23) result in lower equilibrium levels of NO. In the nozzle, equilibrium is maintained until just upstream of the throat, and the NO is reduced to levels ranging from 2.7 to 3.1 mole percent. Downstream from the throat, reaction rates decrease and although free oxygen continues to recombine, the NO mole fraction remains constant.

Comparison With Data

Figure 9 presents for comparison calculated NO levels and experimental values measured at the facility nozzle exit as a function of stagnation enthalpy. The finite rate calculated levels are shown as well as results for assumed conditions of equilibrium in the plenum and frozen flow in the nozzle. Three sources of experimental measurements are presented. The first is from gas samples taken during a series of facility operability tests conducted in 1983 (ref. 6). Samples were collected in bottles through a probe placed at the exit of a metering nozzle installed downstream from the plenum. The sample was then analyzed off-line by a mass spectrometry system. The second source of data is from a series of tests conducted in collaboration with Arnold Engineering Development Center (AEDC) in 1989 (ref. 10) during which NO densities in the AHSTF were measured nonintrusively using a resonance absorption technique. The third source of data (unpublished data obtained by Rocketdyne under the NASP Program, 1992) is from AHSTF tests conducted in 1992 wherein probe samples were collected and analyzed using an on-line mass spectrometry system. Considerable scatter exists in the experimental data at all flight Mach number

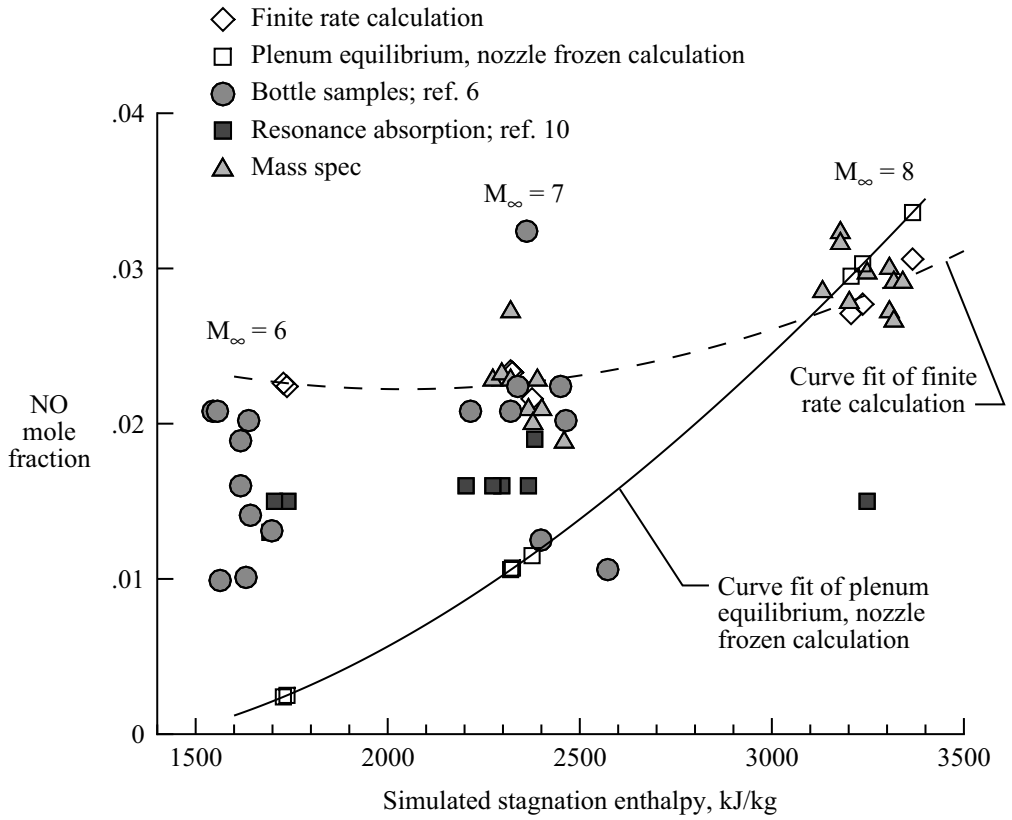

Figure 9. Calculated and experimental NO levels entering facility test section.

simulations. Measurement uncertainties were not provided with the experimental data except for the resonance absorption technique, which quoted an uncertainty of 20 percent. However, despite the large/unknown uncertainties, the finite rate calculated levels show general agreement with the experimental data. Both results of the finite rate analysis and experimental measurements indicate that NO concentrations in the AHSTF are between 1.0 and 3.2 mole percent for the flight simulation range of Mach 6 to 8. Finally, comparison of the equilibrium calculations with the data and finite rate calculations indicates the extent to which the NO level would be underpredicted at the Mach 6 and 7 conditions, if it were assumed that equilibrium is reached in the plenum.

Part II: Effect of NO_x on Engine Performance

Even though the NO concentrations shown in figure 9 are small, the potential effect on scramjet test engine performance could be significant. The effect of NO on ignition delay has been studied both analytically and experimentally (refs. 3 and 11–15); however, because an ignition aid is used in AHSTF engine tests, ignition delay was not investigated in the present study. Instead, the effects of NO on combustion heat release, pressure rise, and engine thrust performance were studied. One premise is that NO_x in the test gas is inert and effectively reduces combustion heat release by trapping some oxygen that would have been available for combustion. Some studies, however, indicate that products of air dissociation, including NO, can enhance combustion heat release (refs. 1 and 2). The latter studies involved a dissociated test gas in a reflected shock tunnel simulating combustor inlet conditions for Mach 17 flight. The effect of NO on scramjet performance depends on the particular combustor inflow conditions; therefore, the effect of NO on the performance of a typical scramjet flow path in the AHSTF was investigated.

For this analytical investigation, the focus was on the Mach 8 simulation for which the NO concentration was the greatest. The calculated facility nozzle exit flow conditions for a Mach 8 simulation were used to define the inflow for a test engine in the AHSTF. The one-dimensional engine analysis model included an inlet compression followed by a combustor process with fuel equivalence ratios of 0.5, 1.0, and 1.5. The overall effect of NO in a Mach 8 simulation was determined by comparing calculated performance using the NO-contaminated air with calculated performance using nondissociated atmospheric air. The nondissociated atmospheric air was defined to have a molar composition of 78.12 percent N_2, 20.95 percent O_2, and 0.93 percent Ar and will hereafter be referred to as nondissociated air.

Analysis

To model the inlet compression process, constraints of a typical subscale model inlet length (127 cm) and throat pressure (≈0.5 atm) for a Mach 8 flight simulation in the AHSTF were imposed. Using the inlet geometry shown in figure 10, oblique shock calculations were performed to obtain a core streamline pressure distribution, also shown in figure 10. Using a conservative curve fit of this pressure distribution, the flow through the inlet was modeled with the one-dimensional finite rate code of reference 8. The inflow was defined by the nozzle exit Mach number ($M_1 = 6$) and the calculated pressure and temperature at the exit of the facility nozzle for the Mach 8 taps 23 simulation (from table 5). These conditions were used for both the Mach 8 taps 23 NO-contaminated air and the nondissociated air. The analysis yielded conditions at the inlet exit that were used as combustor entrance flow conditions. A generic subscale scramjet engine flow path was modeled using a constant-area combustor followed by a nozzle with an expansion ratio of 8. The area distribution for this configuration is shown in figure 11.

The reacting flow in the combustor was modeled using the SCRAM3 code (ref. 1). SCRAM3 is based on the reacting flow codes of references 8 and 9, which solve the differential mass, momentum, energy,

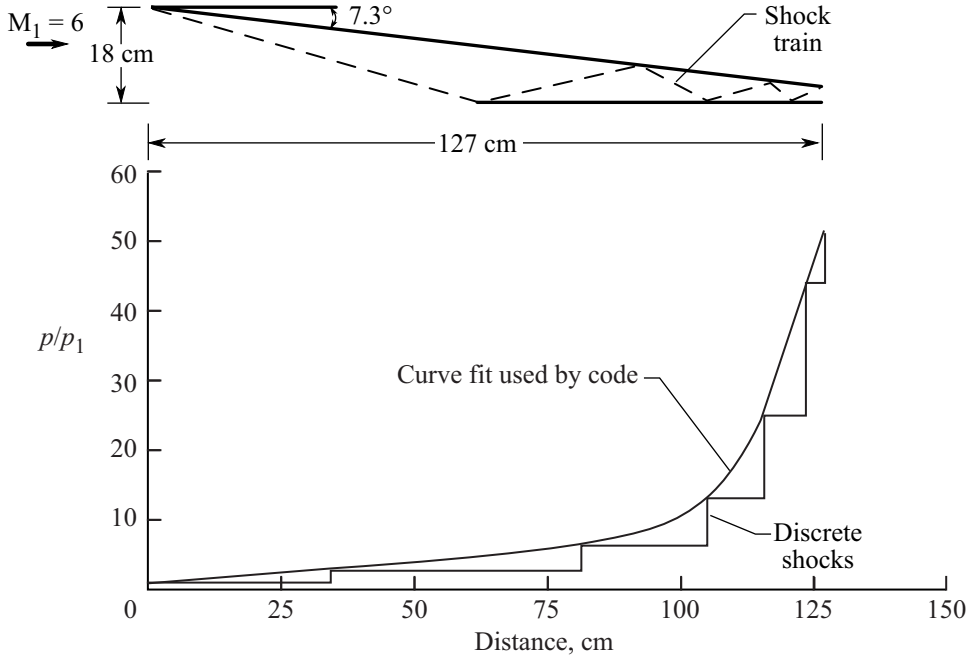

Figure 10. Inlet geometry and pressure distribution for core streamline.

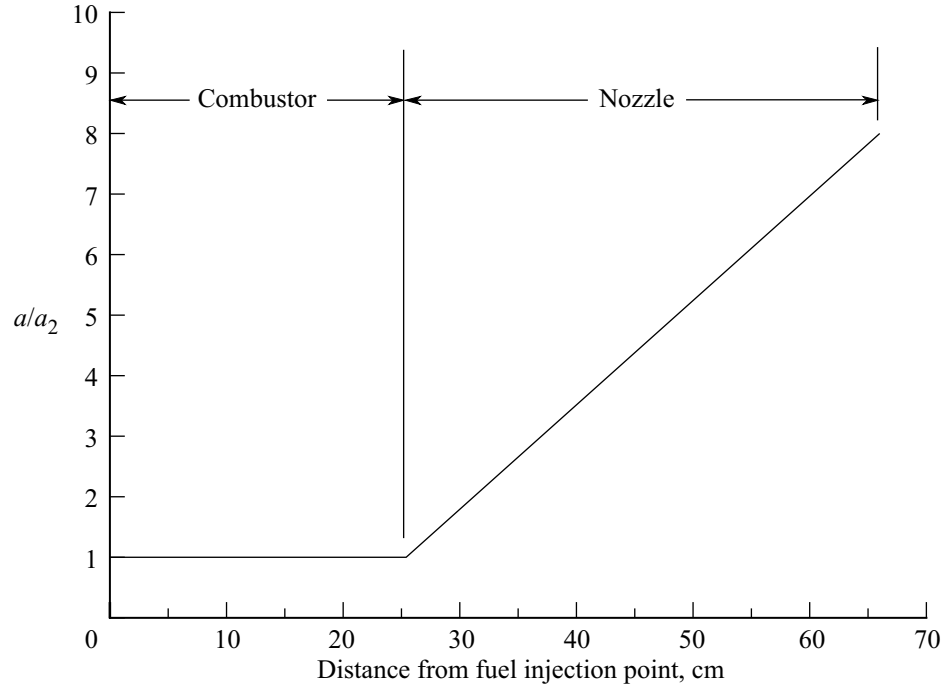

Figure 11. Combustor and nozzle area distribution.

and species conservation equations for a homogeneous mixture of gases at a premixed pressure and temperature. The SCRAM3 code models the fuel, the air, and a reaction zone as three separate streams. A separate initial temperature is assigned to each of the three streams, but they share the same pressure and velocity. The reaction zone volume increases as the fuel and air enter it according to a specified mixing schedule. Average system properties are used in the conservation equations, but the finite rate chemistry equations use the species concentrations and temperature in the reaction zone. An "ignition source" forms the initial reaction zone. It consists of a small percentage of the fuel and air that have been allowed to react to equilibrium at constant pressure and enthalpy. This yields an initial reaction zone with the thermal energy and free radicals necessary to initiate further reactions.

In the AHSTF, a silane-hydrogen mixture (composed of 20 percent SiH_4 and 80 percent H_2 by volume, hereafter referred to as the silane mixture) is used for ignition of the primary hydrogen fuel in test engine combustors. To chemically model the combustion of this fuel mixture with air (containing NO), a reaction mechanism was assembled from two separate mechanisms. The first is the 33-reaction hydrogen-air mechanism listed in table 6. This mechanism was obtained from reference 1 and is based largely on the reaction scheme recommended by the NASP Rate Constant Committee (ref. 16). (However, the rate constant for reaction 24 was altered from ref. 1 to conform with both ref. 16 and the original source, ref. 17.) Note that this hydrogen-air mechanism contains thirteen reactions which allow the NO to take part in the reaction chemistry. The second mechanism is the 35-reaction silane-hydrogen-air model given in table 7. This mechanism, which contains no NO + SiH_xO_y reactions, is based on the silane reaction scheme of reference 18 with modifications recommended by Jachimowski. The full reaction mechanism used in the present study, formed by combining the two mechanisms of tables 6 and 7, was then a 68-reaction mechanism for hydrogen, silane, and air with NO.

Table 6. Hydrogen-Air Reaction Mechanism

Reaction[a]	A	n	E
(1) $H_2 + O_2 \rightarrow HO_2 + H$	7.00×10^{13}	0	56 800
(2) $H + O_2 \rightarrow OH + O$	2.20×10^{14}	0	16 800
(3) $O + H_2 \rightarrow OH + H$	5.06×10^{4}	2.67	6 290
(4) $OH + H_2 \rightarrow H_2O + H$	2.16×10^{8}	1.51	3 430
(5) $OH + OH \rightarrow H_2O + O$	1.50×10^{9}	1.14	0
(6) $H + OH + M \rightarrow H_2O + M$	8.62×10^{21}	−2.0	0
(7) $H + H + M \rightarrow H_2 + M$	7.30×10^{17}	−1.0	0
(8) $H + O + M \rightarrow OH + M$	2.60×10^{16}	−0.6	0
(9) $O + O + M \rightarrow O_2 + M$	1.10×10^{17}	−1.0	0
(10) $H + O_2 + M \rightarrow HO_2 + M$	2.30×10^{18}	−1.0	0
(11) $HO_2 + H \rightarrow OH + OH$	1.50×10^{14}	0	1 000
(12) $HO_2 + O \rightarrow O_2 + OH$	2.00×10^{13}	0	0
(13) $HO_2 + OH \rightarrow H_2O + O_2$	2.00×10^{13}	0	0
(14) $HO_2 + HO_2 \rightarrow H_2O_2 + O_2$	2.00×10^{12}	0	0
(15) $H + H_2O_2 \rightarrow H_2 + HO_2$	1.70×10^{12}	0	3 780
(16) $H + H_2O_2 \rightarrow OH + H_2O$	1.00×10^{13}	0	3 580
(17) $O + H_2O_2 \rightarrow OH + HO_2$	2.80×10^{13}	0	6 400
(18) $OH + H_2O_2 \rightarrow H_2O + HO_2$	7.00×10^{12}	0	1 435
(19) $OH + OH + M \rightarrow H_2O_2 + M$	1.60×10^{22}	−2.0	0
(20) $N + N + M \rightarrow N_2 + M$	2.80×10^{17}	−0.8	0
(21) $N + O_2 \rightarrow NO + O$	6.40×10^{9}	1.0	6 300
(22) $N + NO \rightarrow N_2 + O$	1.60×10^{13}	0	0
(23) $N + OH \rightarrow NO + H$	6.30×10^{11}	0.5	0
(24) $H + NO + M \rightarrow HNO + M$	2.16×10^{15}[b]	0	−600
(25) $H + HNO \rightarrow NO + H_2$	4.80×10^{12}	0	0
(26) $O + HNO \rightarrow NO + OH$	5.00×10^{11}	0.5	0
(27) $OH + HNO \rightarrow NO + H_2O$	3.60×10^{13}	0	0
(28) $HO_2 + HNO \rightarrow NO + H_2O_2$	2.00×10^{12}	0	0
(29) $HO_2 + NO \rightarrow NO_2 + OH$	3.40×10^{12}	0	−260
(30) $HO_2 + NO \rightarrow HNO + O_2$	2.00×10^{11}	0	1 000
(31) $H + NO_2 \rightarrow NO + OH$	3.50×10^{14}	0	1 500
(32) $O + NO_2 \rightarrow NO + O_2$	1.00×10^{13}	0	600
(33) $M + NO_2 \rightarrow NO + O + M$	1.16×10^{16}	0	66 000

[a]Forward reaction rate constants are of the form $k = AT^n e^{-E/RT}$; units are in the cgs system (see nomenclature). Third body efficiencies for all termolecular reactions are 2.5 for M = H_2, 16 for M = H_2O, and 1.0 for all other M.

[b]Rate constant altered from reference 1 to conform with both references 16 and 17.

Three different fueling levels/combinations were analyzed. In each case the silane mixture equivalence ratio was fixed at $\phi_{sim} = 0.15$, as is typical for engine testing in the AHSTF. The equivalence ratios of the primary hydrogen fuel were $\phi_{H_2} = 0.35$, 0.85, and 1.35, resulting in overall or total fuel mixture equivalence ratios of $\phi_{tot} = 0.5$, 1.0, and 1.5. The equivalence ratios were calculated based on the total amount of oxygen in the air, whether in the form of O_2, O, or NO_x.

In the SCRAM3 code, mixing of the fuel and air occurs according to a specified mixing schedule to form a near stoichiometric reaction zone. The mixing schedule is specified as a mixing fraction of the

Table 7. Silane-Hydrogen-Air Reaction Mechanism

Reaction[a]	A	n	E
(1) $SiH_4 \rightarrow SiH_2 + H_2$	9.00×10^{12}	0	52 700
(2) $SiH_2 + O_2 \rightarrow HSiO + OH$	2.20×10^{14}	0	8 000
(3) $SiH_2 + H_2O \rightarrow SiH_2O + H_2$	3.00×10^{12}	0	11 400
(4) $SiH_4 + O_2 \rightarrow SiH_3 + HO_2$	4.00×10^{13}	0	42 800
(5) $SiH_4 + H \rightarrow SiH_3 + H_2$	1.50×10^{13}	0	2 500
(6) $SiH_4 + O \rightarrow SiH_3 + OH$	4.20×10^{12}	0	1 600
(7) $SiH_4 + OH \rightarrow SiH_3 + H_2O$	8.40×10^{12}	0	100
(8) $SiH_4 + HO_2 \rightarrow SiH_3 + H_2O_2$	2.00×10^{12}	0	10 000
(9) $SiH_3 + O_2 \rightarrow SiH_3O_2$	2.00×10^{15}	0	1 200
(10) $SiH_3O_2 \rightarrow SiH_2O + OH$	3.00×10^{12}	0	4 000
(11) $HO_2 + SiH_3O_2 \rightarrow SiH_3O_2H + O_2$	4.00×10^{10}	0	0
(12) $H + SiH_3O_2H \rightarrow SiH_3O_2 + H_2$	4.80×10^{13}	0	7 950
(13) $SiH_3 + O_2 \rightarrow SiH_3O + O$	3.00×10^{12}	0	0
(14) $SiH_3O + O_2 \rightarrow SiH_2O + HO_2$	2.00×10^{12}	0	0
(15) $H + SiH_3 \rightarrow SiH_2 + H_2$	2.00×10^{13}	0	0
(16) $O + SiH_3 \rightarrow SiH_2O + H$	2.00×10^{13}	0	0
(17) $OH + SiH_3 \rightarrow SiH_2O + H_2$	6.00×10^{12}	0	0
(18) $HO_2 + SiH_3 \rightarrow SiH_2 + H_2O_2$	3.00×10^{12}	0	0
(19) $SiH_3 + SiH_3 \rightarrow SiH_2 + SiH_4$	2.00×10^{12}	0	0
(20) $SiH_2O + O_2 \rightarrow HSiO + HO_2$	4.00×10^{14}	0	35 000
(21) $M + SiH_2O \rightarrow HSiO + H + M$	2.00×10^{15}	0	84 500
(22) $H + SiH_2O \rightarrow HSiO + H_2$	3.30×10^{14}	0	10 500
(23) $O + SiH_2O \rightarrow HSiO + OH$	1.80×10^{13}	0	3 080
(24) $OH + SiH_2O \rightarrow HSiO + H_2O$	7.50×10^{12}	0	170
(25) $HO_2 + SiH_2O \rightarrow HSiO + H_2O_2$	1.00×10^{12}	0	12 000
(26) $M + HSiO \rightarrow H + SiO + M$	5.00×10^{14}	0	29 000
(27) $HSiO + O_2 \rightarrow SiO + HO_2$	3.00×10^{13}	0	0
(28) $H + HSiO \rightarrow SiO + H_2$	2.00×10^{14}	0	0
(29) $O + HSiO \rightarrow SiO + OH$	1.00×10^{14}	0	0
(30) $OH + HSiO \rightarrow SiO + H_2O$	1.00×10^{14}	0	0
(31) $HO_2 + HSiO \rightarrow SiO + H_2O_2$	1.00×10^{14}	0	0
(32) $OH + SiO \rightarrow SiO_2 + H$	4.00×10^{12}	0	5 700
(33) $HO_2 + SiO \rightarrow SiO_2 + OH$	1.00×10^{12}	0	0
(34) $O + SiO + M \rightarrow SiO_2 + M$	2.50×10^{15}	0	4 370
(35) $SiO + O_2 \rightarrow SiO_2 + O$	4.00×10^{13}	0	6 500

[a]Forward reaction rate constants are of the form $k = AT^n e^{-E/RT}$; units are in the cgs system (see nomenclature). Third body efficiencies for all termolecular reactions are 1.0 for all M.

form $\eta_m = 1 - e^{-cx}$ where x is the distance from the injection location and c is a constant chosen by the user. For fuel lean or stoichiometric cases ($\phi \leq 1$), η_m is the fraction of total fuel that has mixed and been allowed to enter the reaction zone. For fuel rich cases, it is the fraction of total air that has mixed and been allowed to enter the reaction zone. In the present analysis, the value of the constant c was chosen based on mixing recipes presented in reference 19. Specifically, the value of c was chosen such that, at the exit of the constant area combustor, η_m was equal to the mixing fraction for perpendicular injection from reference 19. This results in combustor exit mixing fractions of η_m = 0.85, 0.70, and 0.80 for

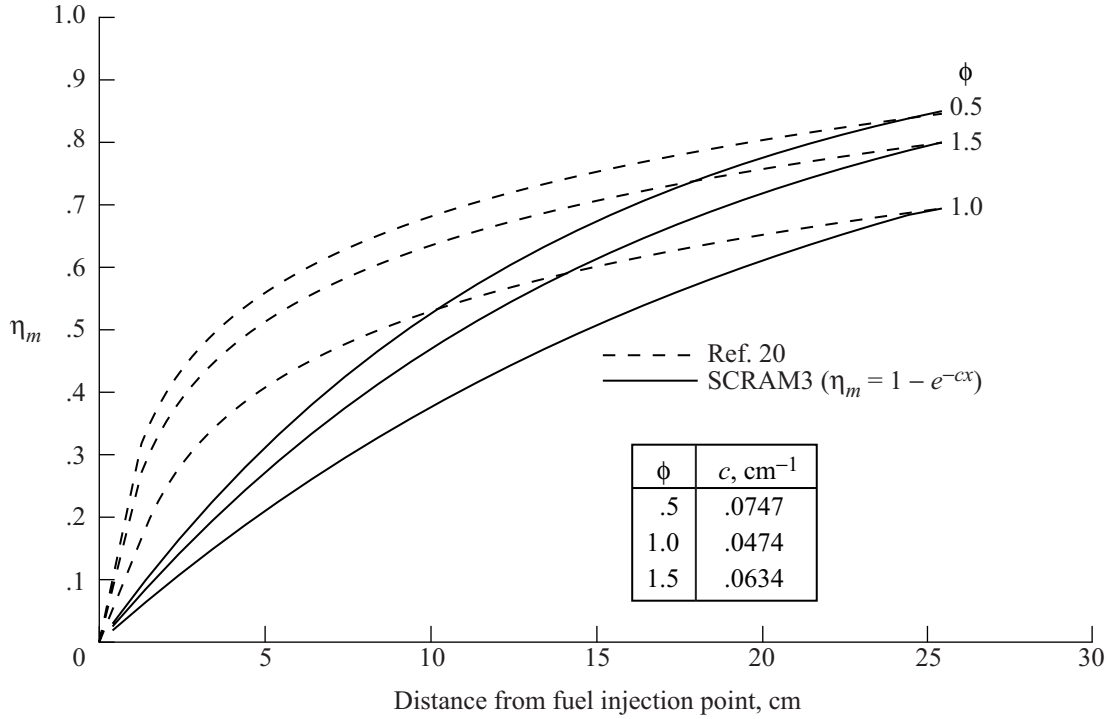

Figure 12. Fuel-air mixing schedules.

ϕ = 0.5, 1.0, and 1.5, respectively. Corresponding mixing schedules are shown in figure 12. Combustion is allowed to continue in the expanding nozzle section.

The initial pressure and velocity assigned to the three streams as well as the temperature assigned to the air stream were those obtained from the inlet analysis described earlier. The fuel stream was assigned a temperature of 300 K and an ignition source created from 2 percent of the overall fuel-air mixture was found to be adequate.

Results and Discussion

Calculations for the flow through the inlet reveal that the composition is frozen for both the nondissociated air and the NO-contaminated test gas. Since the flow is frozen in both cases and the difference between the two test gas compositions is small, then the pressure, temperature, and velocity resulting from the inlet compression process are essentially the same for the two simulations. Table 8 lists the conditions used to define the combustor inflow.

Results of the combustor analysis for the Mach 8 simulation in the AHSTF are presented in figure 13, which compares calculated combustor and nozzle pressure distributions for the NO-contaminated test gas with those for nondissociated air. For each of the three fueling cases, the pressure rise is slightly greater for the NO-contaminated air. The increased pressure is a consequence of the increased chemical energy yield, or heat release (also indicated in fig. 13), for the NO-contaminated air. As noted by Jachimowski in reference 1, NO provides an additional path for the production of water through reactions (24) and (27) of the H_2-air mechanism (table 6) wherein the NO acts as a catalyst:

$$(24) \qquad H + NO + M \rightarrow HNO + M$$

$$(27) \qquad OH + HNO \rightarrow NO + H_2O$$

Table 8. Combustor Inflow Conditions for Mach 8 Flight Simulation

Conditions	Combustor inflow for—	
	Nondissociated air	NO-contaminated air
p, atm	0.477	0.477
T, K	1115	1115
V, m/s	2010	2010
Mole fractions		
N_2	0.7812	0.7659
O_2	0.2095	0.1941
Ar	0.0093	0.0093
NO	0	0.0306
NO_2	0	0.0001

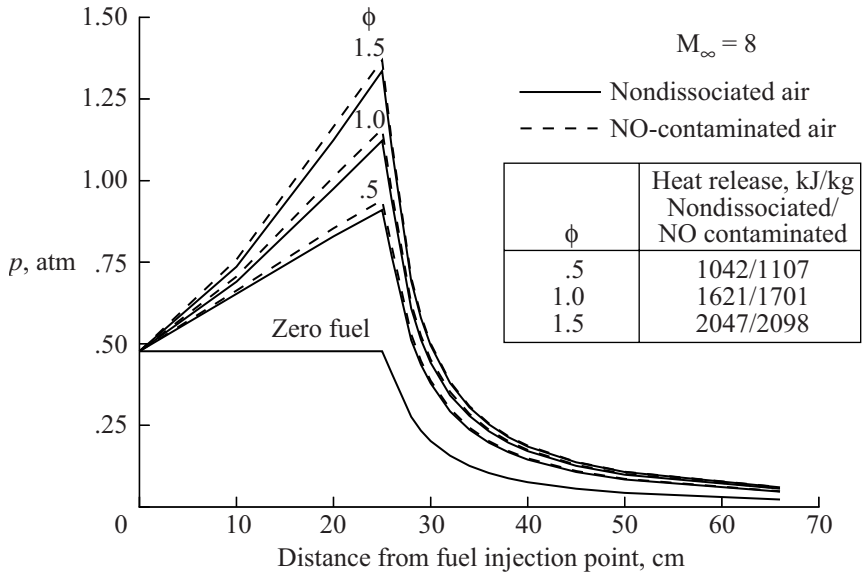

Figure 13. Calculated effect of NO on combustor pressure distributions.

where M is a third body. This reaction pair, wherein NO is consumed then regenerated, serves both to consume free hydrogen and to produce water. Although some of the oxygen that would have been available for reaction is indeed trapped in NO, the heat evolved in H consumption and H_2O production outweighs the deficit caused by the reduced available oxygen. Comparison of the product species shows that combustion with NO-contaminated air results in the same amount of H_2O but less atomic hydrogen. Another factor that contributes to a lesser degree is the reduced level of atomic oxygen in the products for NO-contaminated air, simply due to less available O_2 to dissociate.

To examine the effects of NO in the test gas and verify the importance of reactions (24) and (27), a parametric study was performed for the $\phi = 1.0$ case. Figure 14 presents the combustion heat release distribution for the nondissociated air and the NO-contaminated air using various reaction models. Simulation 1 represents combustion with nondissociated air and simulation 2 represents combustion with

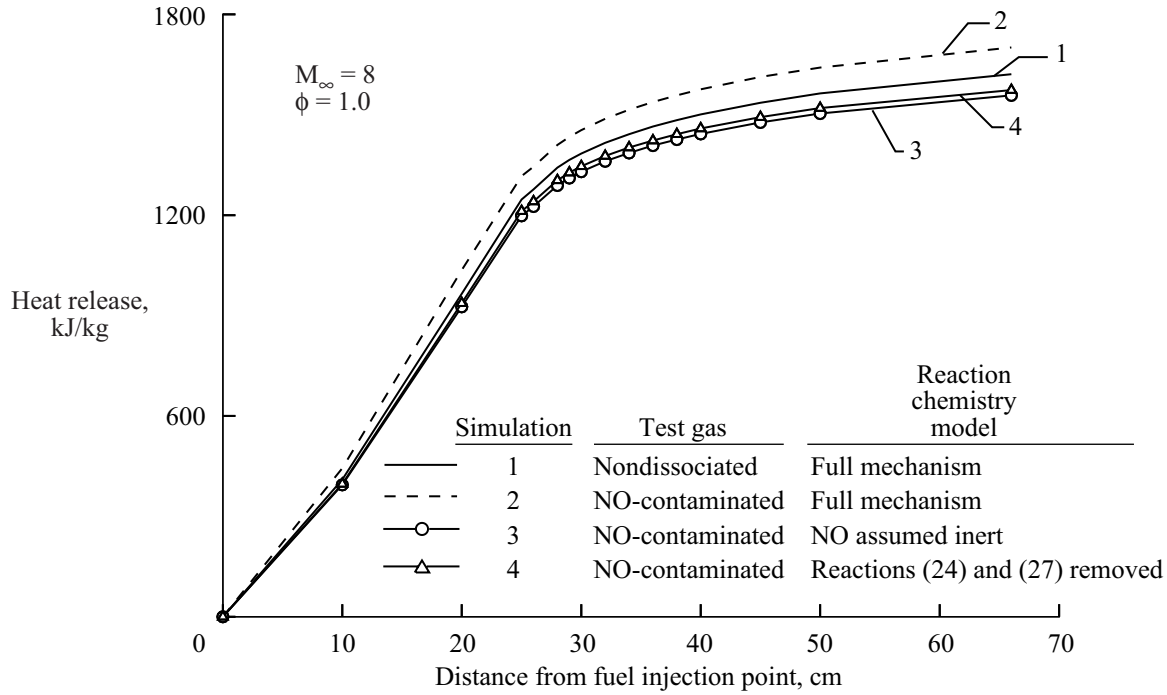

Figure 14. Calculated effect of NO on combustion heat release.

NO-contaminated air, both using the full reaction chemistry model (tables 6 and 7). Comparing the results of these simulations shows the net increase in heat release obtained with NO in the test gas that corresponds to the results shown in figure 13 for $\phi = 1.0$. Simulation 3 represents combustion with NO-contaminated air, but the reaction mechanism was altered by removing all reactions involving NO, in effect making the NO inert. Comparing simulation 3 with simulation 1 shows the expected reduction in heat release because a fraction of the total oxygen is trapped in NO. Comparing simulation 3 with simulation 2 shows the added heat release when the NO is allowed to react. Simulation 4 represents combustion with NO-contaminated air using the full reaction mechanism altered by removing only reactions (24) and (27). Comparing results for simulations 4 and 3 relative to simulation 2 clearly indicates the importance of reactions (24) and (27) to realize the increase in heat release due to the presence of NO.

Ultimately, the effect of NO on measured thrust performance is needed. The performance parameter measured during engine tests is the change in thrust, ΔF, from fuel-off to fuel-on conditions. Assuming that neither the flow in the inlet nor the flow over the external surfaces of the engine change with combustion, ΔF is the change in axial force on the combustor and nozzle due to fuel addition and combustion.

$$\Delta F = F_{\text{fuel on}} - F_{\text{fuel off}} \tag{1}$$

where F is the sum of the combustor and nozzle wall pressure and skin friction forces in the axial direction and the axial fuel momentum. Analytically, the force F can be calculated by applying the momentum equation to the combustor-nozzle control volume. With the assumption of uniform flow, this force can be expressed as:

$$F = (\dot{m}_a + \dot{m}_f) V_e - \dot{m}_a V_2 + p_e a_e - p_2 a_2 \tag{2}$$

where the subscript 2 denotes the combustor entrance and the subscript e denotes the nozzle exit.

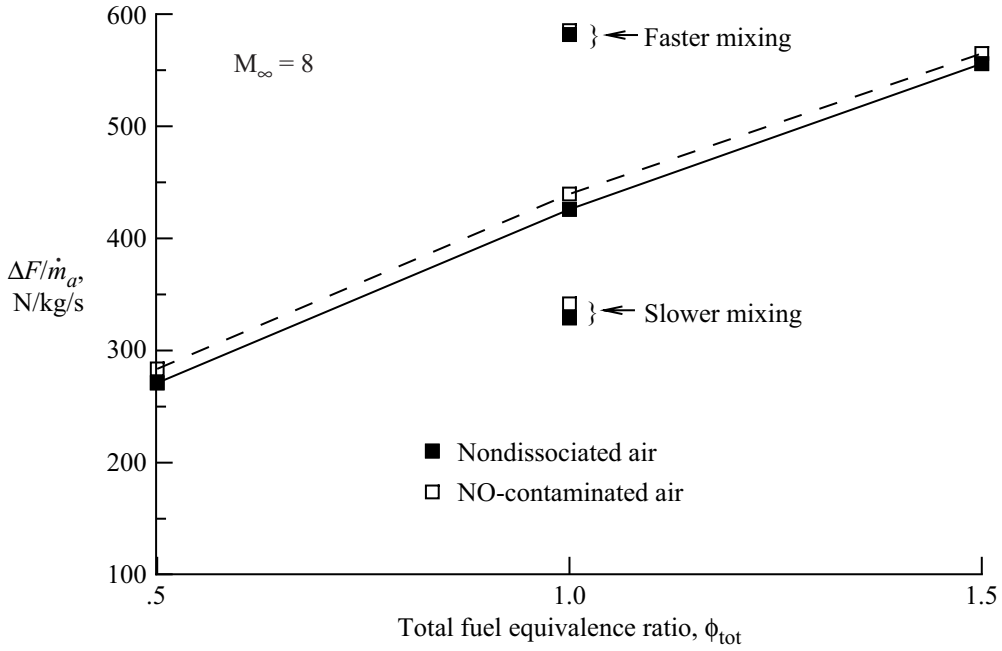

Figure 15. Calculated effect of NO on thrust performance at Mach 8.

In engine tests, the thrust is typically normalized by dividing equation (2) by the mass flow rate of air, $\dot{m}_a$, to compare performance of engines with slightly different mass captures. The resulting parameter, $F/\dot{m}_a$, is the air specific thrust. The SCRAM3 code was used to calculate the air specific thrust for the zero-fuel case and the three fueled cases. Then, the change in specific thrust from fuel-off to fuel-on conditions, $\Delta F/\dot{m}_a$, was computed for each equivalence ratio. The results are summarized in figure 15. The overall effect of the NO on thrust performance is illustrated in this figure, wherein results using the NO-contaminated air are presented for comparison with the results using nondissociated air. The combustion enhancement effect of the NO results in a small increase in the idealized one-dimensional $\Delta F/\dot{m}_a$ ranging from a 4.6-percent increase at $\phi = 0.5$ to a 1.6-percent increase at $\phi = 1.5$.

The sensitivity of the results to the assumed combustor mixing schedule was investigated for $\phi = 1.0$ only using both a slower and faster mixing schedule compared with the assumed schedule of figure 11. Results using combustor exit mixing fractions of $\eta_m = 0.50$ and 0.99 are also shown in figure 15. Although the performance enhancement effect of NO is slightly smaller at the slower and faster mixing rates, the results are not significantly different compared with the results using the assumed $\eta_m = 0.70$.

Although the effect of NO on test engine performance at the Mach 8 simulation is small, the analysis was repeated for the Mach 6 and 7 taps 23 simulations (both had less NO contamination) in order to consider the effects of both the lower static temperatures and higher static pressure of these simulations. The same type of analysis described for the Mach 8 simulation was performed at the Mach 6 and 7 simulations using the NO-contaminated test gas for comparison with nondissociated air. The same generic scramjet flow path geometry was used with the exception that the combustor area ratio was slightly increased to prevent thermal choking. Calculations at the Mach 6 and 7 simulations showed similar trends but with less combustion or thrust enhancement compared with the Mach 8 simulation (see fig. 16). In addition to the smaller levels of NO, the lower temperatures and higher pressures both contribute to diminished effects of NO at the lower Mach number simulations.

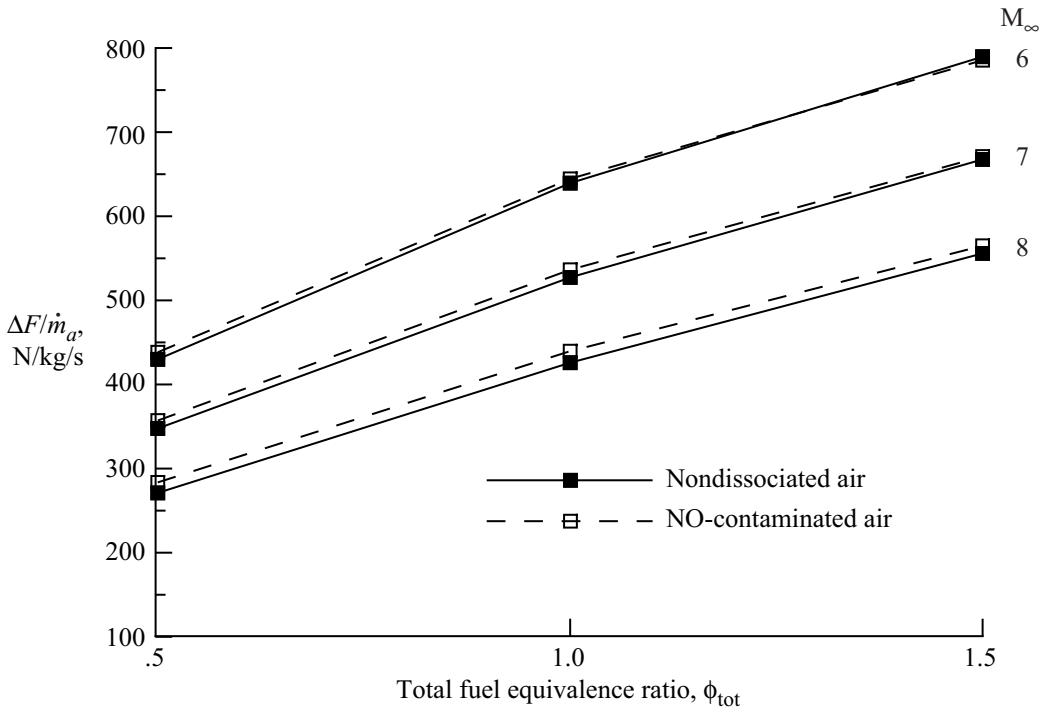

Figure 16. Calculated effect of NO on thrust performance at Mach 6, 7, and 8.

Sensitivity to Rate Constants

An analysis was conducted on the sensitivity of the performance results to the rate constants of selected key reactions in the hydrogen-air mechanism. The selected reactions were (2), (6), (10), (24), and (27) of table 6. Reactions (2) and (10) were chosen because of their importance in the ignition process and reaction (6) for its importance in overall heat release (ref. 20). Reactions (24) and (27) were included owing to their importance when NO is present. For these five reactions, the forward rate constant, k, was varied within the suggested error limits provided in the literature (refs. 17, 21, and 22).

Recommended rate constants and suggested errors for the reactions of interest are listed in table 9. In some sources, errors in the rate constant, k, are quoted as $\Delta \log k = \pm x$, which means there is an uncertainty in k by a factor f, where $\log f = \pm x$ or $f = 10^{\pm x}$. In other sources, the uncertainty is quoted as a factor by $f = \pm x\%$. To perform the uncertainty analysis, the uncertainty factor f was simply applied to the pre-exponential factor A of the forward reaction rate $k = A T^n e^{-E/RT}$. Resulting minimum and maximum values of A are listed in table 10. Note the rate constants used in the present study (table 6) are the same as those listed in table 9 except for reactions (2) and (10), which were modified by Jachimowski to match ignition delay times and laminar flame speeds reported in the literature (ref. 1). However, his modified constants $k_2 = 2.2 \times 10^{14} e^{-16800/\mathrm{RT}}$ and $k_{10} = 2.3 \times 10^{18} T^{-.8}$ are within the recommended error limits (ignoring the small difference in the temperature exponent of reaction (10)).

For the Mach 8, $\phi = 1$ case only, the analysis comparing NO-contaminated air and nondissociated air was repeated using the maximum and minimum values of A (in table 10) to vary the rate constants within the recommended error limits. Initially, the rate constants were varied one at a time for each reaction; subsequently some rate constants were varied simultaneously. Calculations show that varying the rate

Table 9. Recommended Rate Constants and Error Limits

Reaction	Rate constant and error	Reference
(2) $H + O_2 \rightarrow OH + O$	$k = 2.0 \times 10^{14} e^{-16800/RT}$ $\Delta \log k = \pm 0.2$	21
(6) $H + OH + M \rightarrow H_2O + M$	$k = 8.62 \times 10^{21} T^{-2}$ $\Delta \log k = \pm 0.2$	22[a]
(10) $H + O_2 + M \rightarrow HO_2 + M$	$k = 8.4 \times 10^{17} T^{-.8}$ $\Delta \log k = \pm 0.5$	21[b]
(24) $H + NO + M \rightarrow HNO + M$	$k = 2.16 \times 10^{15} e^{600/RT}$ ±50%	17[b]
(27) $OH + HNO \rightarrow NO + H_2O$	$k = 3.6 \times 10^{13}$ ±50%	17

[a]Rate constant adjusted for assumed 3rd body efficiency of 16.25 for H_2O.
[b]Rate constant adjusted for assumed 3rd body efficiency of 2.5 for H_2.

Table 10. Minimum and Maximum Values of Pre-exponential Factor, A, Within Recommended Error Limits for Rate Constants

Reaction	A_{min}	A_{max}
(2) $H + O_2 \rightarrow OH + O$	1.26×10^{14}	3.16×10^{14}
(6) $H + OH + M \rightarrow H_2O + M$	5.43×10^{21}	1.36×10^{22}
(10) $H + O_2 + M \rightarrow HO_2 + M$	2.60×10^{17}	2.65×10^{18}
(24) $H + NO + M \rightarrow HNO + M$	1.08×10^{15}	3.24×10^{15}
(27) $OH + HNO \rightarrow NO + H_2O$	1.80×10^{13}	5.40×10^{13}

constant for reaction (2) makes essentially no difference compared with the previously determined results (i.e., the baseline study using the unmodified constants, simulations 1 and 2 of fig. 14); however, variations in each of the other constants do cause differences. In all cases, the heat release for the NO-contaminated air is still greater than that for the nondissociated air, but the *difference* in heat release (between NO-contaminated and nondissociated air) was made either smaller or larger compared with the baseline study. The difference in heat release is made smaller by either increasing the rate for reactions (6) or (10) or by decreasing the rate for reactions (24) or (27). This is true because increasing k_6 or k_{10} increased the heat release for both test gases but increased it more for the nondissociated air; decreasing k_{24} or k_{27} decreased the heat release for the NO-contaminated air but did not affect the nondissociated air. Likewise, the opposite variation of the constants yields a greater difference in heat release and thrust performance.

Based on the results yielded, it was decided to investigate two limiting cases by a simultaneous variation in the rate constants of reactions (6), (10), (24), and (27), the study of which resulted in the smallest and the largest differences between the NO-contaminated and the nondissociated air. Equivalence ratios of $\phi = 0.5$, 1.0, and 1.5 were included in this part of the study for a direct comparison of thrust results obtained previously with the unmodified constants (as shown in fig. 15). Case A was defined by using

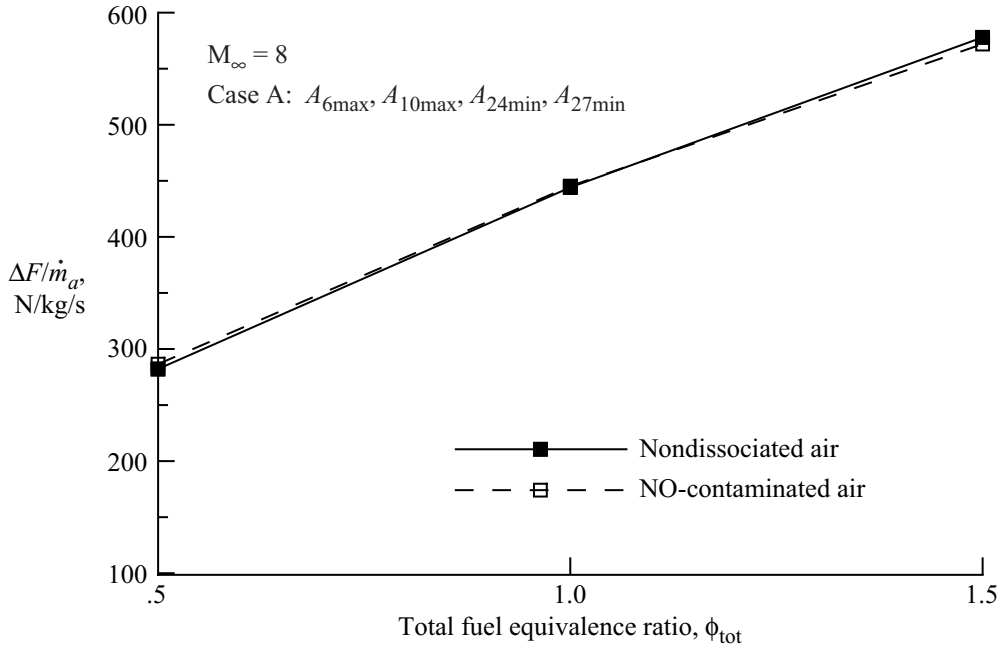

Figure 17. Calculated minimum effect of NO on thrust performance (case A).

the maximum values for the rate constants of reactions (6) and (10) and the minimum values for reactions (24) and (27). As expected, the difference in heat release between NO-contaminated and nondissociated air became smaller and, at $\phi = 1.5$, the actual heat release for the NO-contaminated air became smaller than that for the nondissociated air. The resulting difference in thrust performance is almost negligible as shown in figure 17 where the value of $\Delta F/\dot{m}_a$ for NO-contaminated air relative to nondissociated air ranges from 1.5 percent higher at $\phi = 0.5$ to 1 percent lower at $\phi = 1.5$. Case B was defined by simultaneously using the minimum values for the rate constants of reactions (6) and (10) and the maximum values for reactions (24) and (27). This significantly increased the difference in heat release between the NO-contaminated and nondissociated air, with the NO-contaminated air releasing much more heat. The resulting enhanced thrust performance is shown in figure 18 where the value of $\Delta F/\dot{m}_a$ for NO-contaminated air relative to nondissociated air ranges from 14 to 8 percent higher for $\phi = 0.5$ to 1.5, respectively.

In summary, under Mach 8 simulated conditions in the AHSTF, calculations using the unmodifed rate constants of table 6 indicate a small thrust enhancement of 1 to 5 percent in $\Delta F/\dot{m}_a$ over a range of ϕ's. However, uncertainties in the rate constants of key reactions suggest that the net effect of NO ranges from essentially no effect to an increase in $\Delta F/\dot{m}_a$ of 8 to 14 percent over the same range of ϕ's. Again, to investigate the effects of lower temperature and higher pressure (a lower M_∞ simulation) on the sensitivity of the results to the rate constants, calculations were repeated under the conditions of the Mach 6 simulation for $\phi = 1.0$ only. Results showed the same trends as for the Mach 8 case; the effect of NO ranged from no effect at all to an increase in $\Delta F/\dot{m}_a$ of 5 percent.

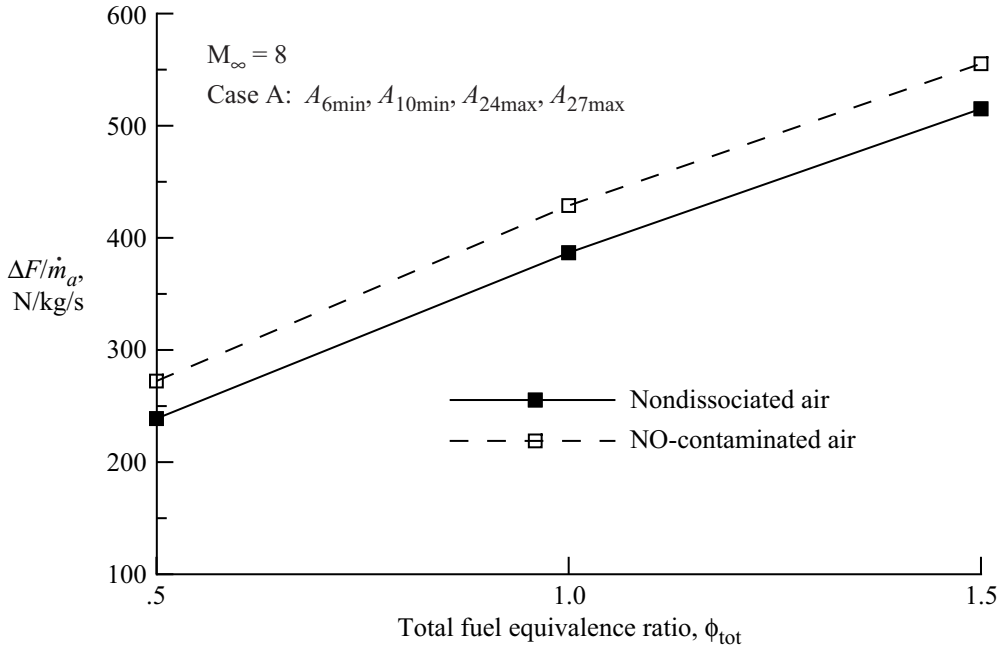

Figure 18. Calculated maximum effect of NO on thrust performance (case B).

Concluding Remarks

This report documents the use of simple engineering tools to evaluate the level of NO and its effect on engine performance in the Langley Arc-Heated Scramjet Test Facility (AHSTF). The levels of nitrogen oxide contamination were quantified analytically over a range of facility operating conditions corresponding to Mach 6, 7, and 8 flight simulations. Modeling the flow one dimensionally, a finite rate kinetics code was used to compute the nitrogen oxide (NO_x) concentration up to the facility nozzle exit. The results showed that the NO_x is primarily composed of nitric oxide (NO), and the calculated NO levels were in general agreement with experimental measurements, indicating NO levels between 1.0 and 3.2 mole percent for flight simulations ranging from Mach 6 to Mach 8, respectively.

The effect of this nitric oxide contamination on hydrogen/air combustion in a scramjet engine flow path was investigated analytically using a three-stream combustor code with finite rate chemistry. The study revealed that, for the Mach 8 simulation, for which the calculated NO levels in the facility were the highest (≈3 mole percent), NO slightly enhances combustion. The deficit in heat release caused by the oxygen bonding in NO is more than offset by an increase in heat release due to the catalytic effect of NO to consume H and produce H_2O. This results in a small increase in one dimensionally calculated thrust performance. The increase in thrust performance ranged from 4.6 to 1.6 percent for total fuel equivalence ratios ranging from 0.5 to 1.5, respectively. Similar calculations showed an even smaller effect of NO at the Mach 6 and 7 simulations.

This study was followed by an uncertainty analysis in which the rate constants of selected key reactions were varied within recommended error limits. The uncertainty analysis suggested that at Mach 8, the net effect of NO in the test gas could range from no effect to an increase in thrust performance on the order of 10 percent over the same range of ϕ's. The uncertainty analysis showed the same trend for the Mach 6 simulation indicating that NO may have no effect or yield a 5-percent increase in thrust performance.

References

1. Jachimowski, C. J.: *An Analysis of Combustion Studies in Shock Expansion Tunnels and Reflected Shock Tunnels*. NASA TP-3224, 1992.

2. Morgan, R.; Stalker, R. J.; Bakos, R. J.; Tamagno, J.; and Erdos, J. I.: Scramjet Testing–Ground Facility Comparisons. ISABE 91-194(L), 1991.

3. MacDermott, W. N.; Horn, D. D.; and Fisher, C. J.: Flow Contamination and Flow Quality in Arc Heaters Used for Hypersonic Testing. AIAA-92-4028, July 1992.

4. Bulewicz, E. M.; and Padley, P. J.: Catalytic Effect of Metal Additives on Free Radical Recombination Rates in $H_2 + O_2 + N_2$ Flames. *Proceedings of the Thirteenth Symposium (International) on Combustion*. The Combustion Institute, 1971, p. 73.

5. Fischer, K. E.; and Rock, K. E.: Calculated Effects of Nitric Oxide Flow Contamination on Scramjet Performance. AIAA-95-2524, July 1995.

6. Thomas, S. R.; and Guy, R. W.: *Expanded Operational Capabilities of the Langley Mach 7 Scramjet Test Facility*. NASA TP-2186, 1983.

7. Guy, R. W.; Torrence, M. G.; Sabol, A. P.; and Mueller, J. N.: *Operating Characteristics of the Langley Mach 7 Scramjet Test Facility*. NASA TM-81929, 1981.

8. McLain, A. G.; and Rao, C. S. R.: *A Hybrid Computer Program for Rapidly Solving Flowing or Static Chemical Kinetic Problems Involving Many Species*. NASA TM X-3403, 1976.

9. Bittker, D. A.; and Scullin, V. J.: *General Chemical Kinetics Computer Program for Static and Flow Reactions, With Application to Combustion and Shock-Tube Kinetics*. NASA TN D-6586, 1972.

10. Howard, R. P.; Dietz, K. L.; McGregor, W. K.; and Limbaugh, C. C.: *Nonintrusive Nitric Oxide Density Measurements in the NASA Langley Arc-Heated Scramjet Test Facility*. AEDC TR-90-29, 1991.

11. Slack, M.; and Grillo, A.: *Investigation of Hydrogen-Air Ignition Sensitized by Nitric Oxide and by Nitrogen Dioxide*. NASA CR-2896, 1977.

12. Rogers, R. C.; and Schexnayder, C. J.: *Chemical Kinetic Analysis of Hydrogen-Air Ignition and Reaction Times*. NASA TP-1856, 1981.

13. Rogers, R. C.: Effects of Test Facility Contaminants on Supersonic Hydrogen-Air Diffusion Flames. *Proceedings of the 23rd JANNAF Combustion Meeting*, 1986.

14. Laster, W. R.; and Sojka, P. E.: Autoignition of H_2-Air: The Effect of NO_x Addition. *Jour. of Propuls.*, vol. 5, no. 4, 1989, pp. 384–390.

15. Lai, H.; and Thomas, S.: Numerical Study of Contaminant Effects on Combustion of Hydrogen, Ethane and Methane in Air. AIAA-95-6097, April 1995.

16. Rate Constant Committee, NASP High Speed Propulsion Technology Team: *Hypersonic Combustion Kinetics*. NASP TM-1107, 1990.

17. Baulch, D. L.; Drysdale, D. D.; and Horne, D. G.: *Evaluated Kinetic Data for High Temperature Reactions, Volume 2: Homogeneous Gas Phase Reactions of the H_2-N_2-O_2 System*. Butterworths, London, 1973.

18. Jachimowski, C. J.; and McLain, A. G.: *A Chemical Kinetic Mechanism for the Ignition of Silane/Hydrogen Mixtures*. NASA TP-2129, 1983.

19. Northam, G. B.; and Anderson, G. Y.: Supersonic Combustion Ramjet Research at Langley. AIAA-86-0159, Jan. 1986.

20. Jachimowski, C. J.: *An Analytical Study of the Hydrogen-Air Reaction Mechanism With Application to Scramjet Combustion*. NASA TP-2791, 1988.

21. Baulch, D. L.; Cobos, C. J.; Cox, R. A.; Esser, C.; Frank, P.; Just, T.; Kerr, J. A.; Pilling, M. J.; Troe, J.; and Walker, R. W.: Evaluated Kinetic Data for Combustion Modelling. *Jour. of Phys. and Chem. Ref. Data*, vol. 21, no. 3, 1992.

22. Gardiner, W. C., editor. *Combustion Chemistry*. Springer-Verlag, New York, 1984.

REPORT DOCUMENTATION PAGE

Form Approved
OMB No. 0704-0188

1. REPORT DATE *(DD-MM-YYYY)*	2. REPORT TYPE	3. DATES COVERED *(From - To)*
01- 05 - 2003	Technical Publication	

4. TITLE AND SUBTITLE
A Finite Rate Chemical Analysis of Nitric Oxide Flow Contamination Effects on Scramjet Performance

5a. CONTRACT NUMBER

5b. GRANT NUMBER

5c. PROGRAM ELEMENT NUMBER

6. AUTHOR(S)
Cabell, Karen F.; and Rock, Kenneth E.

5d. PROJECT NUMBER

5e. TASK NUMBER

5f. WORK UNIT NUMBER
706-51-31-10

7. PERFORMING ORGANIZATION NAME(S) AND ADDRESS(ES)
NASA Langley Research Center
Hampton, VA 23681-2199

8. PERFORMING ORGANIZATION REPORT NUMBER
L-18226

9. SPONSORING/MONITORING AGENCY NAME(S) AND ADDRESS(ES)
National Aeronautics and Space Administration
Washington, DC 20546-0001

10. SPONSOR/MONITOR'S ACRONYM(S)
NASA

11. SPONSOR/MONITOR'S REPORT NUMBER(S)
NASA/TP-2003-212159

12. DISTRIBUTION/AVAILABILITY STATEMENT
Unclassified - Unlimited
Subject Category 07
Availability: NASA CASI (301) 621-0390 Distribution: Standard

13. SUPPLEMENTARY NOTES
Cabell and Rock, Langley Research Center.
An electronic version can be found at http://techreports.larc.nasa.gov/ltrs/ or http://techreports.larc.nasa.gov/cgi-bin/NTRS

14. ABSTRACT

The level of nitric oxide contamination in the test gas of the Langley Research Center Arc-Heated Scramjet Test Facility and the effect of the contamination on scramjet test engine performance were investigated analytically. A finite rate chemical analysis was performed to determine the levels of nitric oxide produced in the facility at conditions corresponding to Mach 6 to 8 flight simulations. Results indicate that nitric oxide levels range from one to three mole percent, corroborating previously obtained measurements. A three-stream combustor code with finite rate chemistry was used to investigate the effects of nitric oxide on scramjet performance. Results indicate that nitric oxide in the test gas causes a small increase in heat release and thrust performance for the test conditions investigated. However, a rate constant uncertainty analysis suggests that the effect of nitric oxide ranges from no net effect, to an increase of about 10 percent in thrust performance.

15. SUBJECT TERMS
Nitric oxide contamination; Vitiation effects; Arc-Heated Scramjet Test Facility; Scramjet engine; Combustion chemistry

16. SECURITY CLASSIFICATION OF:			17. LIMITATION OF ABSTRACT	18. NUMBER OF PAGES	19a. NAME OF RESPONSIBLE PERSON
a. REPORT	b. ABSTRACT	c. THIS PAGE			STI Help Desk (email: help@sti.nasa.gov)
					19b. TELEPHONE NUMBER *(Include area code)*
U	U	U	UU	33	(301) 621-0390